Energy-gain spectroscopy of electron-capture collisions between low-energy Ar and Ne projectiles and atomic and molecular deuterium targets

J. P. Giese, C. L. Cocke, W. Waggoner, and L. N. Tunnell

James R. Macdonald Laboratory, Department of Physics, Kansas State University, Manhattan, Kansas 66506

S. L. Varghese

Department of Physics, University of South Alabama, Mobile, Alabama 36681

(Received 14 April 1986)

Translational energy-gain spectroscopy is used to determine the final-state (nl) populations following single-electron capture by Ar^{q+} $(q = 4-8)$ and Ne^{q+} $(q = 4-7)$ projectiles in atomic and molecular deuterium targets at an energy of $545q$ eV. The importance of kinematics in analyzing these systems is discussed. The final-state populations are found to be very sensitive to the energy-level structure of the collision system. The results are interpreted in terms of a "reaction window" in the energy gain which is calculated using a multichannel Landau-Zener model.

I. INTRODUCTION

One of the fundamental processes occurring in low-energy ion-atom collisions is the transfer of electrons from the target to the projectile. We take "low-energy" collisions to mean those for which the nuclear motion of the projectile is slow compared to the motion of the bound target electrons. At these energies the electrons adjust to the changing interatomic fields and the collision partners form a quasimolecule. Electron capture is generally believed to occur at one or more avoided crossings of the adiabatic potential energy curves of this molecule. Within the last decade, considerable effort has been directed toward collisions between multiply charged ions and hydrogen atoms. These systems provide the simplest test of theory and are also of practical interest in astrophysics and plasma physics.

The emphasis in theoretical research has been on systems with bare projectiles. The potential energy curves of these one-electron systems can be accurately calculated for specific collision partners, which allows detailed study of the charge capture mechanisms. When many-electron projectiles are considered detailed predictions become difficult. However, the large number of curve crossings permits approximations leading to generalized models applicable to many collision systems. Much of the recent experimental work has concentrated on measurement of total electron-capture cross sections for many-electron projectiles. Surveys of these experimental and theoretical efforts are given by Gilbody[1,2] and by Janev.[3] The development of new ion sources has now allowed these measurements to be extended to bare projectiles. A brief review of this work is given by Meyer et al.[4] It should be noted that both the generalized theories and the detailed predictions for specific systems are in reasonable agreement with the experimental data.

A more sensitive test of the theory of electron capture than measurement of the total cross section is the measurement of the final (nl) populations of the projectile. Several groups[5-8] are working in this area with many-electron targets. The initial work in this area for atomic hydrogen targets was done using crossed beam techniques by Stebbings et al.[9] More recently, McCullough et al.[10] and Afrosimov et al.[11] have used translational energy spectroscopy of the charge-changed projectile to determine the energy defect of the final states. The work presented here uses the later method to examine the reactions

$$X^{q+} + D(1s) \rightarrow X^{+(q-1)}(nl) + D^+ , \tag{1}$$

and

$$X^{q+} + D_2(^1\Sigma_g^+) \rightarrow X^{+(q-1)}(nl) \ D_2^{1+}(1s\sigma_g) , \tag{2}$$
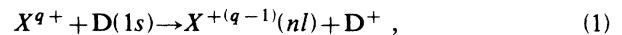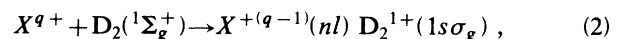
for both argon and neon projectiles at $545q$ eV. We have determined the final (nl) populations for these systems and will compare these results to a multichannel Landau-Zener calculation of the partial cross sections.

II. EXPERIMENT

The present experimental work was performed using the Macdonald Laboratory 6-MV EN tandem Van de Graaff accelerator. The experimental apparatus is shown systematically in Fig. 1. The projectile ions were produced in a secondary recoil ion source based on the design developed by Cocke et al.[12] The recoil cell consisted of a hemispherical electrode and a flat plate electrode. A pump beam of 25-MeV F^{4+} was post-stripped and then passed through the hemispherical electrode. The entrance and exit apertures of this cell were 3 mm in diameter. The recoil target gas was injected into the hemispherical cavity formed by the electrodes. The gas pressure in the cavity caused a rise in the collision chamber pressure to $\sim 6 \times 10^{-7}$ Torr from the background pressure of $\sim 2 \times 10^{-7}$ Torr. The best energy resolution was found experimentally to occur when operating with V_1 close to V_2. The energy of the ions leaving the recoil cell was $E = V_c q$, where the cell potential was given by the empirical formula

$$V_c = V_2 + 0.75(V_1 - V_2) , \tag{3}$$

and q was the charge of the ion. Under normal operating conditions, V_c ranged between 43 and 45 V, with $(V_1 - V_2)$ no longer than 2.5 V.

The ions extracted from the recoil source were directed into the double-focusing magnetic spectrometer with the aid of a set of electrostatic deflectors, $D1$, which operated perpendicular to the magnet plane. The charge- and momentum-analyzed beam emerging from the magnet was directed through the deuterium oven with another set of deflectors, $D2$, also operating perpendicular to the magnet plane.

The atomic deuterium target was produced in a thermal dissociation oven similar in design to that described in detail by Can et al.[13] The heating element of the oven was a tungsten tube, 5.1 cm long and 7.0 mm in diameter, which was rolled out of a 25-μm-thick sheet. Each end of the tube was held between a pair of cylindrical molybdenum sleeves. The outer sleeves were clamped securely in water-cooled copper end plates. The inner sleeves were designed to move longitudinally to allow for thermal expansion of the tungsten tube. The inner sleeves also acted as entrance and exit apertures of 1.5 mm and 4 mm diameter, respectively. The tube was surrounded by a concentric tantalum heat shield and a concentric copper, water-cooled shield. The heating was provided by a half-wave rectified current flowing axially along the tube. The current was rectified to provide a time interval during which energy-gain data could be collected with no voltage drop across the length of the tube. The temperature of the outside of the tube was measured using an optical pyrometer which viewed the tube through a set of holes drilled radially through the heat shields. A heating current of 115 A typically provided a temperature of 2050 K. The suppression of thermionic electrons emerging from the oven was critical and was accomplished by external grids ($S1$ and $S2$) at potentials of -20 V relative to the oven.

The dissociation fraction of D_2 is defined as
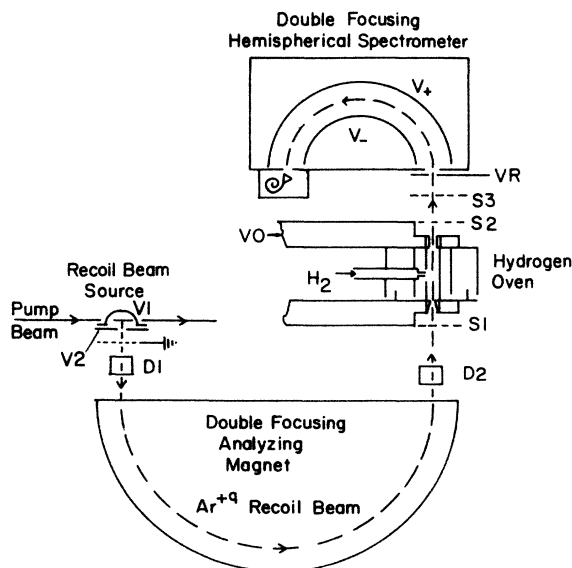
FIG. 1 Schematic of apparatus.

$$ f = \frac{\pi(D)}{\pi(D) + 2\pi(D_2)} = \frac{\alpha}{2 + \alpha} , \tag{4} $$

where $\alpha = \pi(D)/\pi(D_2)$ and $\pi(A)$ is the effective target thickness (particles per area) of molecular or atomic deuterium. As described in detail by Can et al.,[14] α can be determined by measuring the ratio of double-electron-capture events from the D_2 target remaining in the oven at high temperatures to the double-capture events from a pure D_2 target in the cold oven. The large inaccuracies inherent in the use of this method in our case led us to use a more direct method of determining f, as discussed below. The dissociation fraction was determined to be $70 \pm 5 \%$ at 2050 K. When cold, the oven served as a gas cell for argon and molecular deuterium targets. Energy-gain spectra taken as a function of the target pressure for selected cases showed no pressure-dependent features, indicating that single-collision conditions were met.

The collision energy was set by applying a negative potential V_0 to the entire oven assembly. The collision energy is then given by $V_{acc}(q)$, where the effective acceleration potential is $V_{acc} = V_c - V_0$. After passing through grid $S2$, the ions were retarded by applying a voltage V_R to the entrance slit of a hemispherical double-focusing electrostatic spectrometer. The grid $S3$ was used as a focusing element and to keep background electrons in the experimental chamber out of the spectrometer. The spectrometer was operated with a fixed voltage difference $\Delta V = V^+ - V^-$ between the hemispherical plates so that the energy resolution was independent of the energy gain. The energy E of a beam of charge q passing through the spectrometer is given by

$$ E = (V_R + \Delta V/K)q , \tag{5} $$

where K is the spectrometer constant whose measured value was 1.04. After leaving the spectrometer, the ions were accelerated and then detected by a channel electron multiplier.

Energy-gain spectra were collected by scanning the retarding voltage V_R. The data shown here were taken with $V_c = 45.0$ V and $V_0 = -500.0$ V, giving a projectile energy of $545q$ eV. The measured energy resolution of the direct recoil beam which has not undergone charge exchange ranged from $0.25q$ to $0.35q$ eV. The energy gain of a projectile with initial charge q and final charge q' is given by

$$ \Delta E = q'V_R - qV_{R_0} + (q' - q)(\Delta V/K - V_0) , \tag{6} $$

where V_{R_0} is the retarding voltage for which the direct peak is passed.

III. RESULTS AND DISCUSSION

The energy-gain spectra for Ar and Ne projectiles on Ar, D_2 and D targets are shown in Figs. 2—11. The curves in these spectra are drawn to guide the eye. Each peak is labeled with the n and l of the outgoing reaction channel. These outgoing channels and the associated data are presented in Tables I and II.

Although Eq. (6) allows absolute calibration of the energy scale, an observed small dependence of the spectrom-

eter constant K on the focusing led us to favor a calibration based on known energy-gain spectra. We calibrated our spectra for deuterium targets using the final-state populations for Ar^{q+} on Ar systems measured by Nielsen
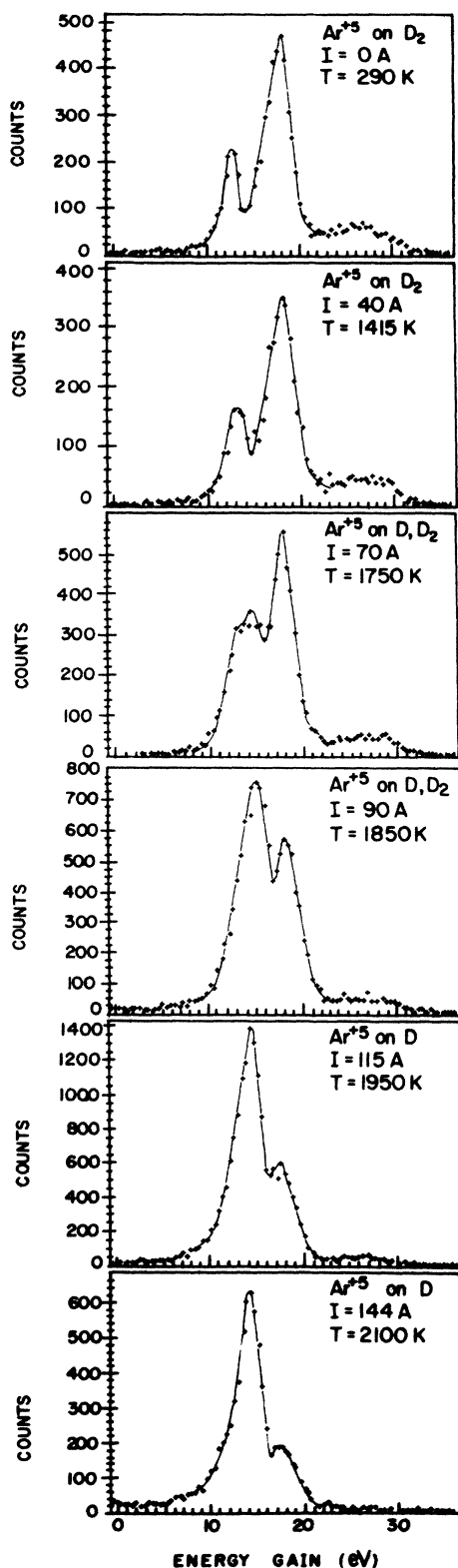
FIG. 2. Energy-gain spectra of Ar^{5+} on D_2 as a function of the oven temperature. The curves are drawn to guide the eye.

et al.[6] All of our data were taken by alternating between deuterium and argon targets without changing any focusing or accelerating voltages. This assured us of a calibration "standard" for each spectrum. We believe the energy scale to be accurate to within ± 0.5 eV. After calibration, the populated final states were identified by comparison of the spectra with the theoretical energy-gain values. The relative probabilities of populating these states were then calculated from $f(nl) = A(nl)/\sum_{n,l} A(nl)$ where $A(nl)$ is the area of the (nl) final state and the sum is over the experimentally observed final states. The areas were determined by a least-squares-fitting program which used a Taylor expansion to calculate the minimum χ^2 for a given fit and the error in the fitting parameters. These errors were used to calculate the error bars for the relative probabilities shown in Tables I and II.
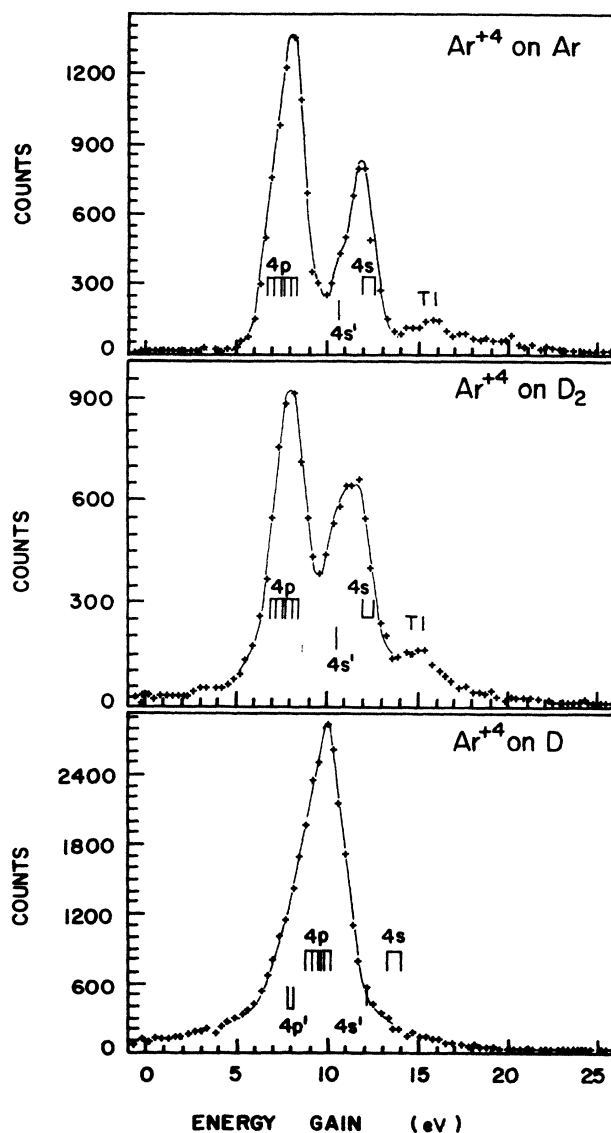
FIG. 3. Energy-gain spectra for Ar^{4+} at 2180 eV on Ar, D_2, and D targets.

A. Kinematics

The energy gain measured for each reaction channel is the difference between the initial energy E_0 and final energy E_f of the projectile. Using classical two-body dynamics[15] the change in energy of the projectile is

$$\Delta E = E_f - E_0 ,$$

$$\Delta E = \left[\frac{M_1}{M_1 + M_2} \right]^2 E_0 \cos^2(\theta)$$

$$\times \left\{ 1 + \left[1 + \frac{M_1(M_1 M_2)}{M_1^2 \cos^2(\theta)} \left[\frac{Q}{E_1} - \frac{M_1}{M_2} + 1 \right] \right]^{1/2} \right\}^2 \tag{7}$$

$$- E_0 ,$$

where M_1 is the projectile mass, M_2 is the target mass, θ is the laboratory scattering angle of the projectile, and Q is the energy defect of the reaction channel. The energy

gain ΔE is equal to the energy defect Q if $Q \ll E_0$, $\theta \simeq 0°$, and $M_1 \simeq M_2$. The last condition is not satisfied for Ar and Ne projectiles on atomic or molecular deuterium targets, where M_1 / M_2 ranges from ~ 5 to 20. The recoil of the target at these mass ratios results in a small but detectable difference between Q and ΔE. We chose to use the more massive deuterium targets instead of hydrogen in order to minimize this effect.

We obtain an estimate of the projectile scattering angle by assuming the projectile follows a classical trajectory through the collision. The electron capture is taken to occur at a localized crossing between the incident and final potential curves. We assume there is no interaction between the collision partners until capture occurs. The collision is then treated as a half Coulomb scattering event with an impact parameter b equal to the crossing radius R_c (a.u. used throughout),

$$b = R_c = (q - 1)/Q . \tag{8}$$

This allows us to calculate a half-Coulomb event angle $\theta_c / 2$ and the energy gain associated with this angle.

The Q values of the possible final states were calculated
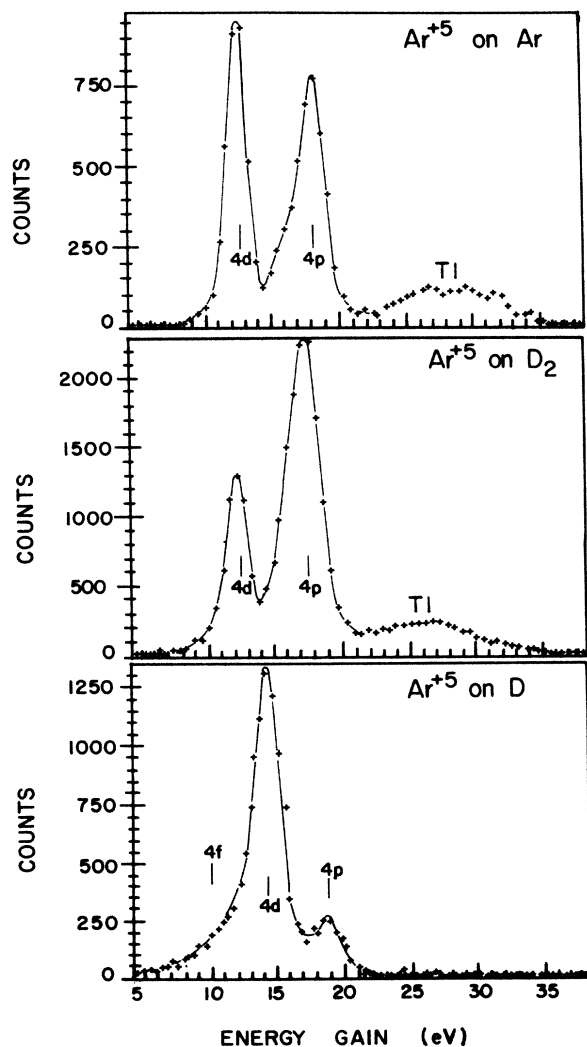
FIG. 4. Energy-gain spectra for Ar^{5+} at 2725 eV on Ar, D$_2$, and D targets.
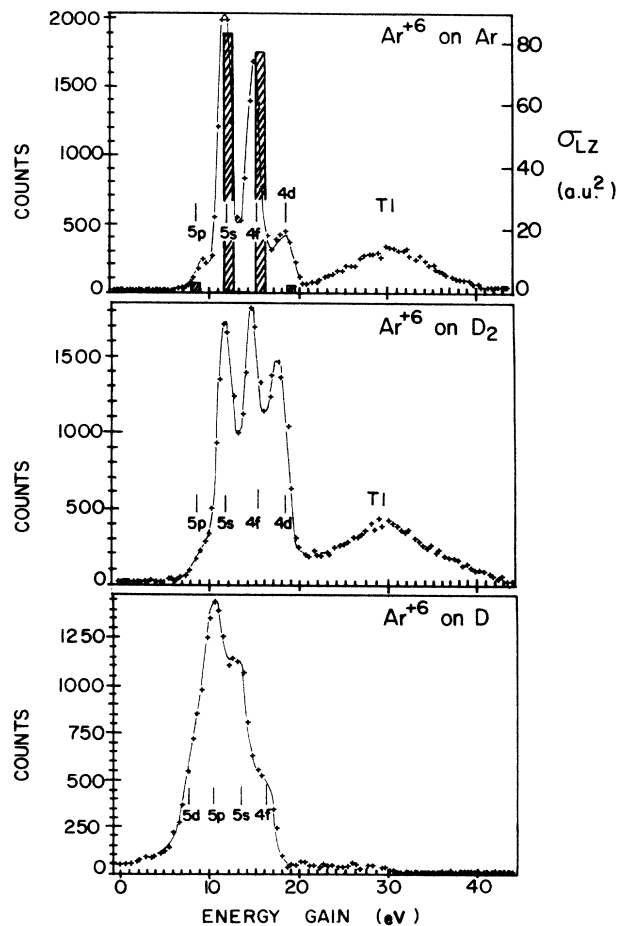
FIG. 5. Energy-gain spectra for Ar^{6+} on Ar, D$_2$, and D targets at 3270 eV. Multichannel Landau-Zener model cross sections for the Ar target are plotted at the approximate Q values of the populated states (see text).

assuming capture occurred without exciting the projectile core and that the product target ion was left in its ground state. The energies of the final states were taken from Bashkin and Stoner[16] when available and otherwise were extrapolated from the isoelectronic sequence following El-Sherbini et al.[17] Our energy resolution was not high enough to resolve any multiplet splitting. In addition, the tabulated values of these splittings are incomplete for highly charged ions. As a result, we have shown individual members of multiplets in Tables I and II only where necessary for the identification of the final states. The values of the energy gain ΔE given in Tables I and II and plotted in Figs. 2—11 were calculated from the Q values assuming a scattering angle of $\theta_c/2$. These scattering angles ranged from 0.071° (1.2 mrad) for $Ar^{6+}+D \rightarrow Ar^{5+}(5d)+D^+$ to 0.227° (3.96 mrad) for $Ar^{5+}+D \rightarrow Ar^{4+}(4p)+D^+$. We believe the sensitivity

of our apparatus to be independent of the scattering angle over this range.

B. Molecular background subtraction

The fraction of an atomic deuterium target which is not dissociated can make significant contributions to the energy-gain spectra. At the operating temperature of our oven, because 15% and 20% of the target, by number density, was molecular. We were able to subtract the molecular background from our atomic deuterium spectra by identifying a two-electron process in the molecular spectra. A common feature of all our spectra for Ar and D_2 targets is a broad peak at high-energy-gain values. Similar features have been identified by Neilsen et al.[6] and Tsurubuchi et al.[18] as due to transfer ionization (TI) processes. Transfer ionization generally refers to any process where the target loses more electrons than the projectile captures. The most likely process for the present collision systems is believed to be capture of two electrons to doubly excited states of the projectiles, which then au-
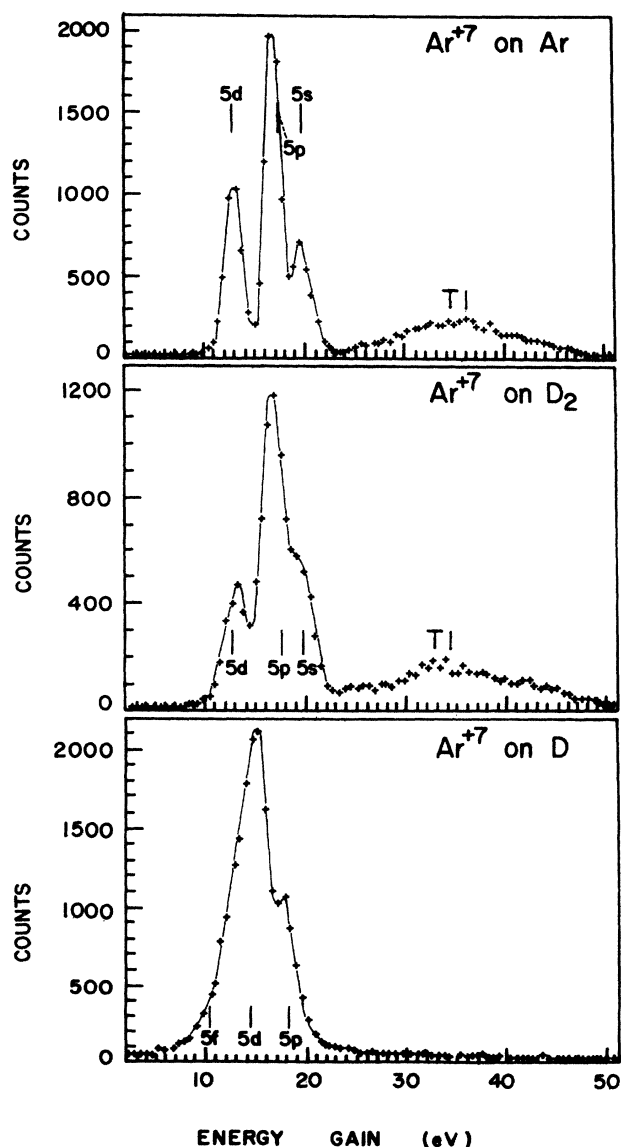
FIG. 6. Energy-gain spectra for Ar^{7+} at 3815 eV on Ar, D_2, and D targets.
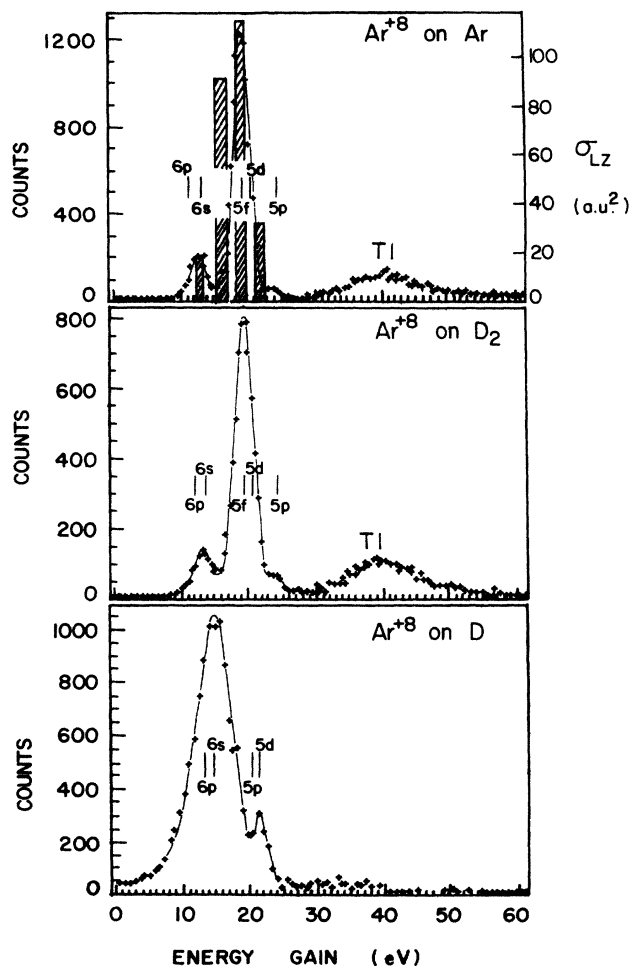
FIG. 7. Energy-gain spectra for Ar^{8+} at 4360 eV on Ar, D_2, and D targets. Multichannel Landau-Zener model cross sections for the Ar target are plotted at the approximate Q values of the populated states (see text).

toionize and are detected in the single-capture spectra.

The transfer ionization peaks seen in the atomic deuterium spectra must be due to molecular background. Except for projectiles with $q = 4$, the transfer ionization peaks were well separated from the single-electron peaks. Thus, it was possible to subtract the molecular background by normalizing to the transfer ionization peaks. As a test of this method, we measured the energy-gain spectra of Ar^{5+} on D_2 as a function of the oven temperature from 290—2100 K. As seen in Fig. 2, the spectrum gradually evolves with increasing temperature, reflecting the change from a molecular target to an atomic target. The raw Ar^{5+} on D spectrum at 2100 K shown in Fig. 2 is consistent with the background-subtracted spectrum shown in Fig. 4. Due to the difficulty in separating the transfer ionization peaks from the single-capture peaks for Ar^{4+} and Ne^{4+} projectiles, the spectra for these projectiles on D were taken at 2100 K and are not background subtracted. The remainder of the spectra for D

targets were taken at 2050 K in order to avoid problems associated with thermal noise in the channeltron.

C. Multichannel Landau-Zener model (MCLZ)

The single-capture cross sections of highly charged projectiles at low energies have been found to be extremely sensitive to the energy-level structure of the projectile and target. Electron capture in the quasimolecular model occurs at localized crossings of the diabatic potential curves of the collision system. The probability of capture occurring at a crossing is low for extremely large or small crossing radii. The range of intermediate crossing radii where the probability of capture is large is called the "reaction window." Several authors[7,19,20] have calculated the location of the reaction window as a function of the crossing radius using the Landau-Zener model. We use this model to interpret the final-state populations by calculating the location of the reaction window in terms of the Q values of the final states.

The Landau-Zener[21,22] probability of a transition between adiabatic curves at a single potential crossing is given by

$$p = \exp(-2\pi H_{12}^2 / v_b \Delta F) , \tag{9}$$
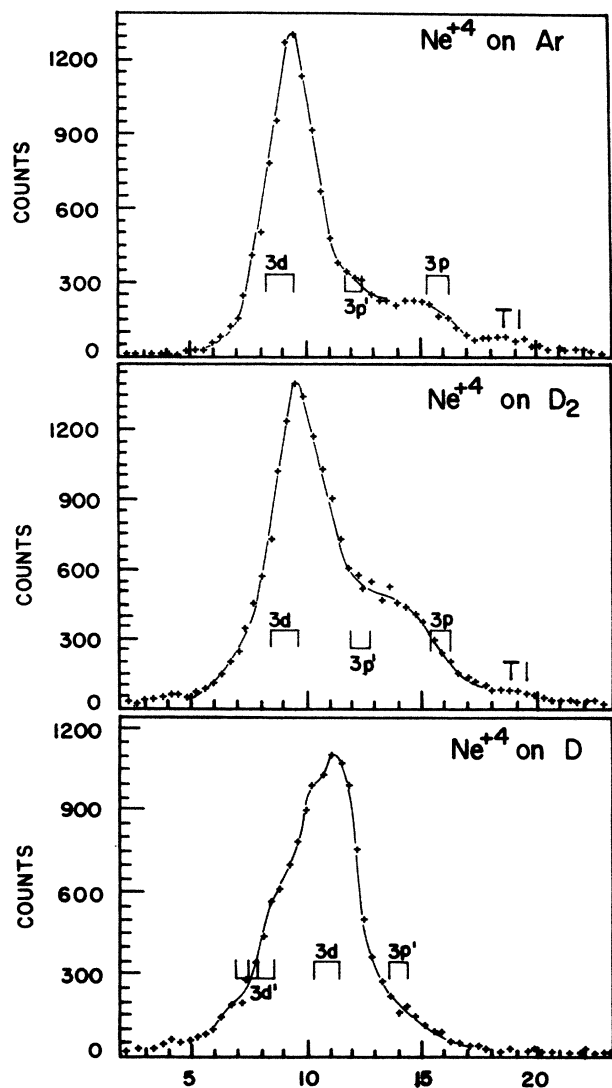
FIG. 8. Energy-gain spectra for Ne^{4+} at 2180 eV on Ar, D_2, and D targets.
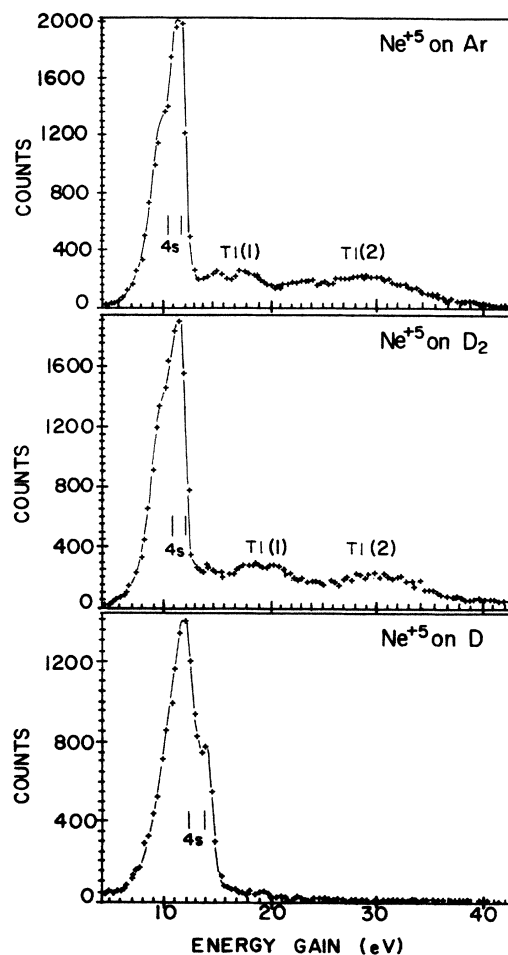
FIG. 9. Energy-gain spectra for Ne^{5+} at 2755 eV on Ar, D_2, and D targets.

where $v_b = v(1-b^2/R_c^2)^{1/2}$ is the radial velocity of the projectile at the crossing, v is the relative velocity, b is the impact parameter, H_{12} is one-half of the adiabatic splitting at the curve crossing, and ΔF is the difference in slopes of the diabatic potential curves at the curve crossing. If the form of the potentials is assumed to be constant with the internuclear separation for the initial channel and a repulsive Coulomb function for the final channel, then it is possible to represent ΔF by

$$\Delta F = (q-1)/R^2 , \tag{10}$$

where q is the charge of the incident projectile. We use the form of the coupling matrix element H_{12} developed by Olson and Salop[23] given by

$$H_{12} = \frac{C_m}{\sqrt{q}} \exp\left[\frac{-1.32\alpha R_c}{\sqrt{q}}\right] , \tag{11}$$

where H_{12} and R_c are in a.u., $\alpha = (2I_t)^{1/2}$, and I_t is the ionization potential of the target atom in a.u. Olson and Salop obtained this form (with the matrix coefficient $C_m = 9.13$) by calculating the potential curves for a large number of fully stripped ions on atomic hydrogen systems and then extending to systems of other targets. However, Kimura et al.[7] reduced this coefficient by 40% in order to achieve agreement with their measurements on He targets. We use C_m as a parameter in fitting this model to our final-state populations. We are aware that other forms of the matrix element H_{12} have been suggested.[24] We have chosen this representation because of its computational simplicity, and we use it as a framework for the qualitative interpretation of our results.

When there is only one crossing, the total probability of the electron transfer at a given impact parameter is given by
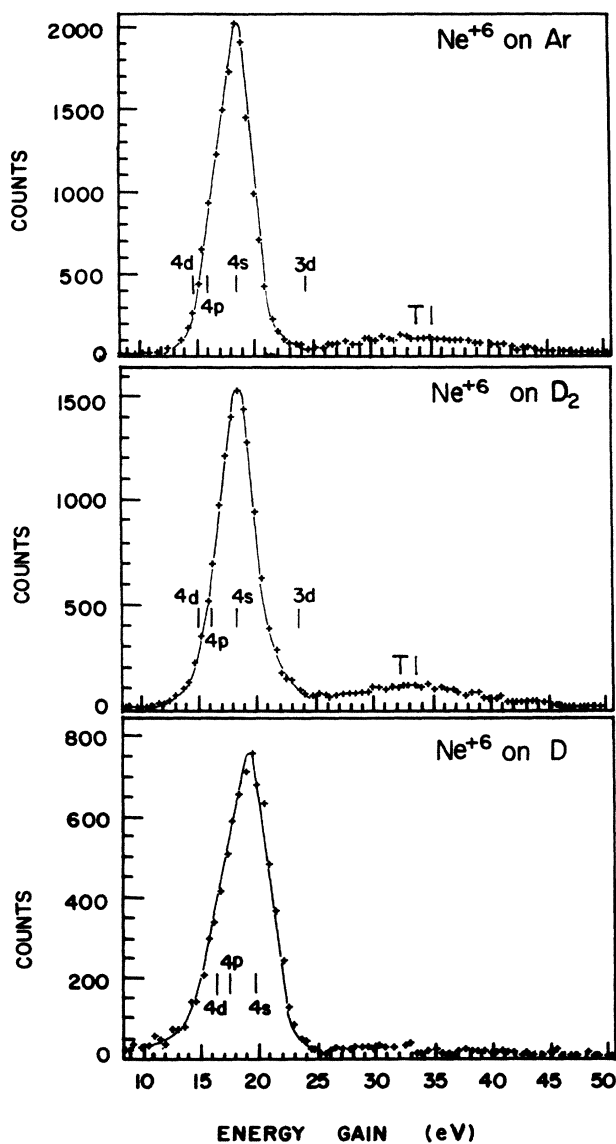
FIG. 10. Energy-gain spectra for Ne^{6+} at 3270 eV on Ar, D$_2$, and D targets.
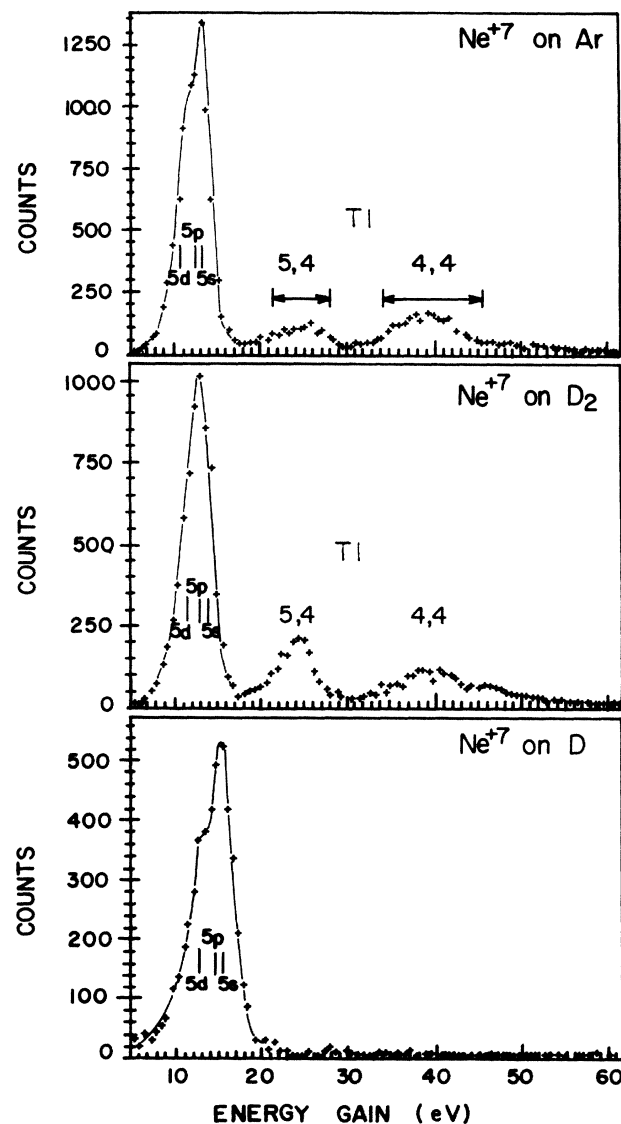
FIG. 11. Energy-gain spectra for Ne^{7+} at 3815 eV on Ar, D$_2$, and D targets.

TABLE I. Summary of collision parameters for Ar^{q+} on Ar, D_2, and D targets at $545q$ eV. Only populated energy levels and the associated relative probabilities, f_{nl}, deduced from the present data, are shown. The energy gains ΔE were calculated from the Q values correcting for kinematic shifts (see text).

Projectile	Final state	Ar ΔE (eV)	Ar $f_{n,l}$	D₂ ΔE (eV)	D₂ $f_{n,l}$	D ΔE (eV)	D $f_{n,l}$
Ar^{4+}	$3s^23p^2(^3P)4s(^4P)$	12.91	0.256±0.031	12.85	0.281±0.052	14.04	0.055±0.007
	(^2P)	12.22		12.19		13.43	
	$(^1D)4s\,(^2D)$	10.80	0.062±0.027	10.85	0.115±0.052	12.29	0.024±0.005
	$(^3P)4p\,(^4D)$	8.52	0.569±0.020	8.67	0.466±0.017	10.16	0.771±0.018
	(^4P)	8.17		8.33		9.84	
	(^2D)	7.99		8.15		9.68	
	(^4S)	7.90		8.06		9.58	
	(^2P)	7.40		7.57		9.12	
	(^2S)	6.93		7.12		8.70	
	$(^1D)4p\,(^2P)$					8.16	0.150±0.010
	(^2D)					7.93	
	TI		0.112±0.024		0.139±0.014		
Ar^{5+}	$3s^23p4p$	17.98	0.402±0.039	17.73	0.545±0.036	18.72	0.140±0.009
	$4d$	12.70	0.365±0.030	12.72	0.219±0.012	14.09	0.668±0.025
	$4f$					9.79	0.192±0.018
	TI		0.234±0.016		0.236±0.038		
Ar^{6+}	$3s^24d$	18.87	0.086±0.003	18.66	0.255±0.010		
	$4f$	15.07	0.282±0.006	15.05	0.230±0.012	16.37	0.123±0.011
	$5s$	11.87	0.308±0.007	11.97	0.237±0.007	13.25	0.277±0.022
	$5p$	8.50	0.040±0.003	8.69	0.029±0.002	10.33	0.413±0.030
	$5d$					7.71	0.187±0.017
	TI		0.284±0.003		0.278±0.009		
Ar^{7+}	$3s5s$	20.15	0.152±0.008	19.95	0.191±0.024		
	$5p$	17.16	0.360±0.012	17.10	0.332±0.030	18.38	0.187±0.013
	$5d$	12.79	0.200±0.013	12.88	0.146±0.013	14.38	0.678±0.028
	$5f$					10.40	0.135±0.016
	TI		0.288±0.012		0.331±0.023		
Ar^{8+}	$2p^65p$	24.23	0.015±0.002	24.00	0.022±0.004		
	$5d$	20.37	0.617±0.018	20.22	0.527±0.027	21.42	0.068±0.009
	$5f$	19.11		19.03		20.25	
	$6s$	13.07	0.106±0.005	13.16	0.097±0.013	14.69	0.932±0.038
	$6p$	11.33		11.49		13.06	
	TI		0.261±0.032		0.354±0.061		

$$P = 2p(1-p) . \qquad (12)$$

The general expression for N states and $N-1$ crossings is

given by Salop and Olson[25] assuming that there is no interference between different paths leading to a particular final state. The probability for capture into the ith final state is

$$P_i = p_1p_2 \cdots p_i(1-p_i)[1+(p_{i+1}p_{i+2} \cdots p_N)^2+(p_{i+1}p_{i+2} \cdots p_{N-1})^2(1-p_N)^2$$

$$+(p_{i+1}p_{i+2} \cdots p_{N-2})^2(1-p_{N-1})^2+ \cdots +p_{i+1}^2(1-p_{i+2})^2+(1-p_{i+1})^2] . \qquad (13)$$

The partial cross section σ_i is obtained by integrating over the impact parameter. The total cross section is then found by summing over the possible final states. We have not attempted to account for the possibility of rotational coupling between the final states. Janev et al.[26] have included rotational coupling in the MCLZ model for bare

projectiles on atomic hydrogen. However, there is no simple extension of their model to many-electron projectiles.

We have calculated the partial and total cross sections for each of the collision systems. As can be seen from Eqs. (9)—(11) the probability for capture depends on the charge of the projectile and on the Q value of the final

TABLE II. Summary of collision parameters for Ne^{q+} on Ar, D_2, and D targets at $545q$ eV. Only populated energy levels and the associated relative probabilities, f_{nl}, deduced from the present data, are shown. The energy gains ΔE were calculated from the Q values correcting for kinematic shifts (see text).

Projectile	Final state	Ar ΔE (eV)	Ar $f_{n,l}$	D_2 ΔE (eV)	D_2 $f_{n,l}$	D ΔE (eV)	D $f_{n,l}$
Ne^{4+}	$2p^2(^3P)3p(^4P)$	16.28	0.137±0.022	16.29	0.113±0.035		
	(^4S)	15.25		15.30			
	$(^1D)3p(^2F)$	12.50	0.136±0.039	12.63	0.332±0.139	14.18	0.116±0.009
	(^2D)	11.79		11.94		13.52	
	$(^3P)3d(^4P)$	9.48	0.692±0.067	9.68	0.533±0.196	11.34	0.525±0.024
	(^2D)	8.33		8.55		10.24	
	$(^1D)3d(^2F)$					8.28	
	(^2D)					7.84	0.359±0.020
	(^2P)					7.42	
	(^2S)					6.96	
	TI		0.034±0.004		0.022±0.007		
Ne^{5+}	$3p4s(^3P)$	11.83	0.361±0.015	11.88	0.362±0.019	13.66	0.211±0.016
	(^1P)	10.60	0.220±0.010	10.69	0.325±0.017	12.48	0.789±0.035
	TI(1)		0.125±0.007		0.246±0.024		
	TI(2)		0.295±0.022		0.157±0.022		
Ne^{6+}	$3s^23d$	24.07		23.96			
	$4s$	18.12	0.565±0.031	18.19	0.679±0.022	19.68	0.787±0.033
	$4p$	15.63	0.243±0.018	15.75	0.151±0.011	17.33	0.213±0.017
	$4d$	14.54		14.68		16.29	
	TI		0.192±0.033		0.170±0.010		
Ne^{7+}	$2s5s$	13.44		13.62		15.29	0.543±0.041
	$5p$	12.44	0.727±0.030	12.64	0.645±0.022	14.33	
	$5d$	10.94		11.15		12.85	0.457±0.041
	TI(5-4)		0.096±0.012		0.171±0.010		
	TI(4-4)		0.178±0.015		0.184±0.011		

state [through Eq. (8)]. When Q_i is too small H_{12} is so small that p is near unity and P is negligible. Similarly, when Q_i is very large H_{12} is also very large, p is small, and P is again negligible. Thus there is a reaction window in Q value where the probability of capture has an appreciable magnitude. The width and location of the reaction window are dependent on C_m and on the density of final states. A single state calculation therefore will not accurately reflect the position of the reaction window. We fit the theoretical partial cross sections to our final-state populations by adjusting this coefficient. The actual distribution in Q value of resolvable final states for each collision system was approximated for the model calculations by a uniform density of states. As an example, consider the case of Ar^{6+} on Ar (Table I) where the Q values 8.60, 12.03, 15.46, and 18.89 eV were used to represent the $5p$, $5s$, $4f$, and $4d$ final states instead of the actual values of 8.50, 11.87, 15.07, and 18.87 eV. The theoretical partial cross sections for this example are plotted in Fig. 5 in histogram form. As another example, partial cross sections are also plotted for Ar^{8+} on Ar in Fig. 7.

The fitted values of C_m for each target and projectile are given in Table III along with the calculated and experimental (where available) total cross sections. The Landau-Zener cross sections tend to slightly overestimate the experimental values, but the degree of agreement is

reasonable given that the form of the coupling matrix element was developed for bare projectiles on atomic hydrogen. We believe this indicates the model is applicable to these systems. The values of C_m are in most cases less than that used by Olson and Salop.[23] This is expected because the coefficient given there, 9.13, represents coupling to the only parabolic state which, for a given n, can couple to the incident channel. The l-subshell degeneracy is removed in our cases by the departure of the projectile core from a point charge. Thus, the amplitude of the parabolic state is spread over spherical states of different l but the same n. The coupling matrix coefficient for hydrogenic projectiles reflects the projection of these spherical states onto the parabolic state.[27] The situation is more complicated for the multielectron projectiles we use because the final states on the projectile are no longer degenerate in the principal shell. However, a similar projection is possible,[27] with the C_m for individual (nl) states dependent on the energy of the state. The average effective C_m which we find in our fitting procedures should be reduced as a result of this projection. It is perhaps surprising that C_m is not even smaller than we find.

The values of C_m for D_2 are always lower than those for Ar, possibly due to the larger number of electrons on the Ar target. Another possible explanation for this effect is the population of excited vibrational levels of the D_2^+

TABLE III. A comparison of matrix coupling coefficients (C_m), total Landau-Zener cross sections σ_{LZ}, and experimental cross sections σ_{expt} for Ar and Ne projectiles on Ar, D_2, and D targets. All cross sections are given in units of 10^{-15} cm^2. Experimental cross sections for Ar targets are from Ref. 6, D_2 from Ref. 13, D with Ar projectiles from Ref. 32, and D with Ne projectiles from Ref. 33.

$q+$		Ar	D_2	D
		Neon		
4	C_M	3.54	3.05	3.05
	σ_{LZ}	2.25	2.31	2.50
	σ_{expt}		3.20	2.05
5	C_M	12.0	9.80	6.16
	σ_{LZ}	4.56	4.56	4.74
	σ_{expt}		3.60	4.0
6	C_M	2.88	2.59	1.74
	σ_{LZ}	4.32	4.29	4.28
	σ_{expt}		3.70	
		Argon		
4	C_M	6.30	5.05	4.55
	σ_{LZ}	3.26	3.23	3.53
	σ_{expt}		3.20	3.10
5	C_M	2.7	1.65	1.80
	σ_{LZ}	3.54	3.18	3.62
	σ_{expt}		2.62	3.2
6	C_M	9.53	4.65	10.25
	σ_{LZ}	4.55	4.34	4.89
	σ_{expt}	7.11	4.2	4.3
7	C_M	7.45	5.75	6.89
	σ_{LZ}	5.37	5.25	6.85
	σ_{expt}	5.01	5.23	4.5
8	C_M	7.88	6.65	8.25
	σ_{LZ}	7.15	7.07	8.13
	σ_{expt}	4.62	4.89	5.5

target. Several authors have suggested accounting for this effect by multiplying H_{12} by the square root of the Frank-Condon factor when molecular targets are used. However, we point out that the Frank-Condon factor represents the overlap between well-defined vibrational states. Our energy resolution is not sufficient to resolve individual vibrational levels. Therefore, it is not clear *a priori* that these factors should be included in our calculations.

No other consistent trends are seen as either the projectile charge or target is varied. At its present state of complexity, this model is most useful in the interpretation of final-state populations. The predictive abilities could be improved by calculating the coupling matrix H_{12} for each state of a specific collision system. Such a calculation has been carried out by Larsen and Taulbjerg[28] for Ar^{6+} on H using quantum-defect wave functions in a close-coupling model. Calculations using their results indicate the strongest final populations should be in the $4f$ and $5s$ states, in slight disagreement with our results showing strongest population in the $5s$ and $5p$ states. The large kinematic shifts associated with the light deuterium target make it possible in principle to misidentify the populated

states. In order to investigate this point, we made experimental measurements of the differential cross sections[29] for Ar^{6+} incident on D_2. The results show that the angular distributions are centered closer to the Coulomb scattering angle θ_c than to the half Coulomb event angle which we assumed in our kinematic calculations. However, even at these larger projectile scattering angles, the kinematic shifts are consistent with our initial identifications. Thus the disagreement between theory and experiment appears unresolved.

D. Discussion

Our spectra indicate the the final populations are determined primarily by the energetics of the collision system rather than by the nature of the target, whether it be atomic, molecular, many electron, or one electron. The spectra for argon and molecular deuterium are very similar, with the same (nl) values populated. This similarity can be attributed to the small difference between the binding energies of Ar (15.75 eV) and molecular deuterium (15.43 eV). Further comparison of these spectra, within the limit of our energy resolution, does not reveal any clear evidence of vibrational excitation of the molecular deuterium target during the capture process. A direct Frank-Condon transition would lead to significant population of the $v=0$ through about the $v=13$ vibrational levels[30] of D_2^+, covering an energy range of approximately 2 eV. The resulting shift and broadening of the single-capture peaks are not present in our spectra. We are led to the conclusion that the present collision velocities are not sufficiently high to produce a strict Frank-Condon transition, and that the internuclear distance partially relaxes during the collision. One can understand this conclusion by calculating the ratio of the collision time T_c ($\simeq 2R_c/v$) to the time necessary for the D_2^+ molecule to move to its equilibrium internuclear separation T_r ($\simeq \frac{1}{4}$ of a vibrational period). This ratio ranges from $T_c/T_r = 1.04$ to 1.92, indicating that the molecule should have time to substantially relax. It should be noted that capture into the first vibrational level of D_2^+ results in a shift to lower Q value of 0.2 eV. This shift is of the same magnitude and in the same direction as the kinematic shifts discussed above. Thus, it would be difficult to distinguish population of the first few vibrational states from the expected kinematic shift.

Comparison of the spectra for atomic and molecular deuterium targets for cases where the density of states is large (Ar^{q+}, $q = 5-8$) reveals a shift of the reaction window to smaller energy gains for the atomic target. Within the context of the MCLZ model, this occurs in part because of the lower binding energy of the atomic target through the factor α in Eq. (11). We point out that a further increase of the coupling matrix element through an increase in C_m is required to fit the data for the atomic targets. While the reaction window is shifted to lower energy gains by the decrease in the binding energy of the atomic target, the Q value of a given final state is shifted to higher values. As a result, the final-state populations for the atomic targets are shifted to slightly higher l values compared to the molecular cases.

The possibility of metastable contamination of the projectile beam must be considered for multiply charged ions. Only for the cases of Ar^{4+} and Ne^{4+} projectiles were we required to use metastable projectile cores in order to identify populated states. The electron configuration for both projectiles is np^2 which gives the mestastable levels ^1D and ^1S in addition to the ground state ^3P. Our resolution is not high enough to determine the metastable fraction of the incident beam for either of these cases. However, it is clear that some of the final-state population is due to capture to the ^1D metastable state.

The positive identification of the broad, high-energy-gain peaks as due to TI processes depends on knowledge of the doubly excited states which are populated prior to autoionization. The energy levels of these states are generally not known, but reasonable numerical estimates can be made. Consider the specific system $Ne^{7+} + Ar$ $\rightarrow (Ne^{5+})^{**} + Ar^{2+}$. Energy levels for configurations of the form (nl,n',l') were calculated from a Hartree-Fock program by Wilson.[31] The range of energy gains accessible to these levels is shown in Fig. 11. The double capture appears to be into states of the form $(5l,4l')$ or $(4l,4l')$. It is impossible to identify exactly which states are populated due to the kinematic broadening of the TI peak caused by recoil of the projectile following ejection of the autoionizing electron.

A common feature of all our spectra for Ar and D_2 targets is the similarity in the energy-gain values of the TI peaks. This appears to imply that the energy required to remove two electrons from D_2 is nearly the same as that for Ar (43.39 eV). However, the energy needed to remove the two electrons from D_2 depends on the charge-capture mechanism. If both electrons are removed simultaneously in a Frank-Condon transition, then the energy required to remove both electrons is 50.94 eV. This would place the TI peaks for D_2 targets at Q values 7.55 eV lower than for Ar if the same final states are populated. If the electrons are removed adiabatically with the molecular ion allowed to completely relax as the electrons are removed, then the required energy is 31.67 eV and the TI peaks should come 11.72 eV higher in Q value than for the Ar target. The kinematic effects due to the difference in target masses must also be considered. The lighter D_2 target will be scattered with larger recoil energy than for the Ar target, resulting in lower energy gains for the projectile. However, these kinematic shifts are expected to be a few eV, substantially less than the 11.72 eV difference in Q value. As noted for single capture, this analysis suggests that the capture process at these projectile velocities is in the intermediate region between a Frank-Condon transition and an adiabatic transition.

The D_2^{2+} molecular ion must lose 7.55 eV through relaxation of the internuclear separation during the double-capture process, if the Q values for TI from the Ar and D_2 targets are to agree. An estimate of the time T_R needed for this relaxation, made by assuming that the Coulomb force between the deuterons is constant over the relaxation time, gives $T_R = 1.5 \times 10^{-15}$ sec. The ratio

T_c/T_R of the collision time to the relaxation time for our systems ranges from 3.51 to 6.54. Thus, there is ample time for the molecule to relax during the collision.

It is possible that the double-capture process populates different final states on the projectile with D_2 and Ar targets, and that the similarity in the TI spectra for the two targets is imposed by similar effective reaction windows for two electron transfer. However, pronounced structure in the TI spectra is seen for the cases of Ne^{5+} and Ne^{7+} which we identify with population of particular groups of final states as indicated in Figs. 9 and 11. The relative location of the TI groups for Ar and D_2, for these cases at least, must directly reflect the two electron separation energies for the two targets. Thus we believe it unlikely that significantly different final states are populated for the two targets in other cases.

IV. CONCLUSIONS

The final state populations following charge capture are very sensitive to the energy-level structure of the collision systems. The differences in the populated states between the Ar, D_2, and D targets can be attributed to shifts in the reaction window for capture caused by the different strengths of the effective coupling matrix elements. Significant population of transfer ionization peaks is seen for both Ar and D_2 targets. The similarity in the energy gains for the TI peaks for these targets indicates that the two-electron-capture process from the molecular target is in the intermediate region between a Frank-Condon transition and an adiabatic transition. A similar conclusion is reached for single capture from D_2 from the absence of evidence for strong vibrational excitation. The MCLZ model adequately describes the relative populations of the final states with reasonable values for the coupling matrix elements. The model seems to be more useful as an interpretive rather than predictive tool in analyzing these collision systems. The prediction of final state populations awaits more sophisticated calculation of the coupling matrix elements H_{12} and incorporation of rotational coupling effects.

[1] H. B. Gilbody, Nucl. Instrum. Methods Sci. 214, 109 (1983).

[2] H. B. Gilbody, Phys. Scr. 23, 143 (1981); 24, 712 (1981).

[3] R. K. Janev, Comments At. Mol. Phys. 12, 277 (1983).

[4] F. W. Meyer, A. M. Howald, C. C. Havener, and R. A. Phaneuf. Phys. Rev. A 32, 3310 (1985).

[5] R. Mann, C. L. Cocke, A. S. Schlachter, M. Prior, and R. Marrus, Phys. Rev. Lett. 49, 1329 (1982).

[6] E. H. Nielsen, L. H. Andersen, A. Barany, H. Cederquist, J. Heinemeier, P. Hvelplund, H. Knudsen, K. B. MacAdam, and J. Sorensen, J. Phys. B 18, 1789 (1985).

[7] M. Kimura, T. Iwai, Y. Kaneko, N. Kobayashi, A. Matsumoto, S. Ohtani, K. Okuno, S. Takagi, H. Tawara, and S. Tsurubuchi, J. Phys. Soc. Jpn. 53, 2224 (1984).

[8] B. A. Huber and H. J. Kahlert, J. Phys. B 16, 4655 (1983).

[9] R. F. Stebbings, R. A. Young, C. L. Oxley, and H. Erhardt, Phys. Rev. 138, A1312 (1965).

[10] R. W. McCullough, F. G. Wilike, and H. B. Gilbody, J. Phys. B 17, 1373 (1984).

[11] V. V. Afrosimov, A. A. Baselaev, K. O. Lzhkin, and M. N. Panov, Abstracts of Contributed Papers, Thirteenth International Conference on the Physics of Electronic and Atomic Collisions, Berlin, 1983, edited by J. Eichler, W. Fritsch, I. V. Hertel, N. Stolterfoht, and U. Willie (North-Holland, Amsterdam, 1983), p. 546.

[12] C. L. Cocke, R. Dubois, T. J. Gray, and E. Justiniano, IEEE Trans. Nucl. Sci. NS-28, 1032 (1981).

[13] C. Can, T. J. Gray, J. M. Hall, L. N. Tunnell, and S. L. Varghese, IEEE Trans. Nucl. Sci. NS-30, 943 (1983).

[14] C. Can, T. J. Gray, S. L. Varghese, J. M. Hall, and L. N. Tunnell, Phys. Rev. A 31, 72 (1985).

[15] J. B. Marion and F. C. Young, Nuclear Reaction Analysis Graphs and Tables (American Elsevier, New York, 1968), p. 142.

[16] S. Bashkin and J. O. Stoner, Jr., Atomic Energy-Level and Grotrian Diagrams (North-Holland, Amsterdam, 1975).

[17] T. M. El-Sherbini, A. Salop, E. Blocmen, and F. J. deHeer, J. Phys. B 13, 1433 (1980).

[18] S. Tsurubuchi, T. Iwai, Y. Kaneko, M. Kimura, N. Kobayashi, A. Matsumoto, S. Ohtani, K. Okuno, S. Takagi, and H. Tawara, J. Phys. B 15, L733 (1982).

[19] H. Cederquist, L. H. Andersen, A. Barany, P. Hvelplund, H. Knudsen, E. H. Nielsen, J. O. Pedersen, and J. Sorensen, J. Phys. B 18, 3951 (1985).

[20] F. W. Meyer, A. M. Howald, C. C. Havener, and R. A. Phaneuf. Phys. Rev. Lett. 54, 2663 (1985).

[21] L. Landau, Phys. Z. Sowjetunion 2, 46 (1932).

[22] C. Zener, Proc. R. Soc. London Ser. A 137, 696 (1932).

[23] R. E. Olson and A. Salop, Phys. Rev. A 14, 579 (1976).

[24] R. K. Janev and L. P. Presnyakov, Phys. Rep. 70, 1 (1981).

[25] A. Salop and R. E. Olson, Phys. Rev. A 13, 1312 (1976).

[26] R. K. Janev, D. S. Belic, and B. H. Bransden, Phys. Rev. A 28, 1293 (1983).

[27] K. Taulbjerg (private communication).

[28] O. G. Larsen and K. Taulbjerg, J. Phys. B 17, 4523 (1984).

[29] L. N. Tunnell, C. L. Cocke, W. T. Waggoner, and J. P. Giese, Abstracts of Contributed Papers, Fourteenth International Conference on the Physics of Electronic and Atomic Collisions, Palo Alto, 1985, edited by M. J. Coggiola, D. L. Heustis, and R. P. Saxon (ICPEAC, Palo Alto, 1985), p. 472.

[30] D. Villarejo, J. Chem. Phys. 49, 2523 (1968).

[31] M. Wilson (private communication).

[32] D. H. Crandall, R. A. Phaneuf, and F. W. Meyer, Phys. Rev. A 22, 379 (1980).

[33] W. Seim, A. Muller, I. Wirkner-Bott, and E. Salzborn, J. Phys. B 14, 3475 (1981).